Striations in the Taurus molecular cloud: Kelvin–Helmholtz instability or MHD waves?

M. Heyer, P. Goldsmith, U. Yildiz, R. Snell, E. Falgarone, J. Pineda

Monthly Notices
of the
ROYAL ASTRONOMICAL SOCIETY

MNRAS **461,** 3918–3926 (2016)
Advance Access publication 2016 June 30

doi:10.1093/mnras/stw1567

Striations in the Taurus molecular cloud: Kelvin–Helmholtz instability or MHD waves?

M. Heyer,[1]⋆ P. F. Goldsmith,[2] U. A. Yıldız,[2] R. L. Snell,[1] E. Falgarone[3] and J. L. Pineda[2]

[1]*Department of Astronomy, University of Massachusetts, Amherst, MA 01003, USA*
[2]*Jet Propulsion Laboratory, 4800 Oak Groave Drive, Pasadena, CA 91109, USA*
[3]*LERMA, CNRS UMR 8112, Ecóle Normale Supeŕieure, 24 rue Lhomond, F-75231 Paris Cedex 05, France*

Accepted 2016 June 28. Received 2016 June 28; in original form 2016 March 30

ABSTRACT

The origin of striations aligned along the local magnetic field direction in the translucent envelope of the Taurus molecular cloud is examined with new observations of ^{12}CO and ^{13}CO J = 2−1 emission obtained with the 10-m Submillimeter Telescope of the Arizona Radio Observatory. These data identify a periodic pattern of excess blue and redshifted emission that is responsible for the striations. For both ^{12}CO and ^{13}CO, spatial variations of the J = 2−1 to J = 1−0 line ratio are small and are not spatially correlated with the striation locations. A medium comprised of unresolved CO emitting substructures (cells) with a beam area filling factor less than unity at any velocity is required to explain the average line ratios and brightness temperatures. We propose that the striations are generated from the modulation of velocities and beam filling factor of the cells as a result of either the Kelvin–Helmholtz instability or magnetosonic waves propagating through the envelope of the Taurus molecular cloud. Both processes are likely common features in molecular clouds that are sub-Alfvénic and may explain low column density, cirrus-like features similarly aligned with the magnetic field observed throughout the interstellar medium in far-infrared surveys of dust emission.

Key words: MHD – turbulence – waves – ISM: kinematics and dynamics – ISM: magnetic fields – ISM: molecules.

1 INTRODUCTION

Supersonic gas motion in Galactic molecular clouds is a key property that determines cloud evolution and the production of newborn stars. The observed gas motions are most generally attributed to turbulent flows in a medium with very large Reynolds number, which reflects the ratio of inertial to viscous forces. The variation of velocity dispersions with spatial scales in molecular clouds strongly supports the presence of turbulent flows in these regions (Larson 1981; Falgarone, Puget & Perault 1992; Heyer & Brunt 2004). Since the interstellar magnetic field threads molecular clouds, any description of gas motions and cloud structure must consider the role of the magnetic force.

Arons & Max (1975) attributed the supersonic line widths to hydromagnetic waves and derived three conditions for such waves to operate: (1) magnetic stress larger than the thermal gas pressure, (2) a weak field limit such that field fluctuations, δB are much smaller than the static field, $B_\circ$, and (3) wave period longer than the neutral–ion collision time that couples the neutral material to the magnetic field. Subsequent theoretical studies have further explored the role of hydromagnetic waves in molecular clouds (Langer 1978; Carlberg & Pudritz 1990; Mouschovias 1991; Gehman, Adams & Watkins 1996; Basu & Dapp 2010) with a recent comprehensive treatment provided by Mouschovias, Ciolek & Morton (2011).

Hydromagnetic instabilities can also imprint structure to the velocity and density fields of interstellar clouds. Specifically, the Kelvin–Helmholtz (K-H) instability can develop from density inhomogeneities and velocity shear layers from turbulent or champagne-like flows. The density perturbations generated by the instability may account for some of the complex structure found in molecular clouds (Berné & Matsumoto 2012; Hendrix, Keppens & Camps 2015).

A valuable target to examine the role of the magnetic field in cloud motions is the translucent envelope of the Taurus molecular cloud. ^{12}CO J = 1−0 imaging of the cloud identified a network of faint, narrow, elongated features, hereafter, called striations, that are aligned along the local magnetic field direction (Goldsmith et al. 2008). Heyer et al. (2008) analysed the ^{12}CO and ^{13}CO J = 1−0 emission from a subfield of the most prominent striations and found distinct velocity structure functions along axes parallel and perpendicular to the local field direction. That is, gas

⋆ E-mail: heyer@astro.umass.edu

velocities vary smoothly, if at all, along the magnetic field direction but exhibit higher spatial frequency differences transverse to the field. Such magnetically aligned velocity anisotropy is evident in magnetohydrodynamic (MHD) simulations only when the motions are sub-Alfvénic and the magnetic pressure is larger than the local thermal pressure (Heyer et al. 2008). The plane of the sky component of the magnetic field in this region of the Taurus cloud has been estimated by Chapman et al. (2011) to be 12–37 μG based on the Chandrasekhar–Fermi effect (Chandrasekhar & Fermi 1953).

In this study, we present new ^{12}CO and ^{13}CO J = 2−1 line emission data from the most prominent striations in the Taurus cloud. These observations have higher angular resolution and much higher signal-to-noise ratios than the CO J = 1−0 data presented by Goldsmith et al. (2008) that surveyed much of the Taurus cloud complex. The new data also enable an examination of the excitation conditions. In Section 2, the collection of these new data is described. The results are presented in Section 3, along with a summary of velocity variations and line excitation analysis. In Section 4, we examine the K-H instability and magnetosonic waves as the responsible agents for the appearance and kinematics of the striations.

2 DATA

The Arizona Radio Observatory (ARO) 10-m Submillimeter Telescope on Mount Graham was used to observe the J = 2−1 transitions of ^{12}CO and ^{13}CO towards a subfield in the Taurus molecular cloud that exhibited bright filamentary features in the ^{12}CO J = 1−0 images presented by Goldsmith et al. (2008). Observations were made on 2014 November 28–December 1, 2015 January 28–29, and 2015 February 9–18. The front end was the ALMA Band 6 prototype receiver, which has the capability for simultaneous dual polarization observations of ^{12}CO 2–1 in the upper side band and ^{13}CO 2−1 in the lower side band. The spectrometers were filter banks with 250 kHz resolution corresponding to 0.325 and 0.341 km s^{-1} at 230 and 220 GHz, respectively. The beam size at the ^{12}CO 2−1 line frequency is 32 arcsec.

The observed field was centred on coordinates, RA(J2000) = $04^{h}48^{m}48\overset{s}{.}29$, Dec(J2000) = $26^{\circ}39'58\overset{''}{.}5$. The map was constructed from 14 subfields, each 10 arcmin ×10 arcmin in extent, using the 'On-the-Fly' (OTF) scanning method. To increase the signal-to-noise ratio, each subfield was observed two to four times.

Routines within GILDAS[1] were applied to convolve the irregularly sampled OTF data with a Gaussian kernel with 10 arcsec half-power beam width to yield a final Nyquist-sampled map. The data were acquired on the $T_{\rm A}^{*}$ antenna temperature scale and scaled up to main beam temperatures using the beam efficiency of 0.74 for both J = 2−1 transitions. The achieved median 1σ rms sensitivity in main beam temperature units for both ^{12}CO and ^{13}CO is 0.11 K.

We also make use of the Taurus ^{12}CO and ^{13}CO J = 1−0 data collected by the Five Colleges Radio Astronomy Observatory 14-m telescope (Narayanan et al. 2008). These data have higher native spectral resolution but less sensitivity as these are part of the larger survey of the Taurus molecular cloud. The J = 1−0 data have also been corrected for the error beam pattern of the 14-m telescope so the antenna temperatures correspond to main beam temperature units. To facilitate a comparison with the two data sets, all data were smoothed to an angular resolution (HPBW) of 50 arcsec and a velocity spacing of 0.325 km s^{-1}. The median 1σ rms sensitivities of these smoothed data are 0.04 and 0.03 K for ^{12}CO and ^{13}CO J = 2−1 and 0.46 and 0.24 K for ^{12}CO and ^{13}CO J = 1−0.

[1] http://www.iram.fr/IRAMFR/GILDAS

3 RESULTS

The ^{12}CO J = 1−0 data of the Taurus striations presented by Goldsmith et al. (2008) demonstrate that these features are spatially coherent within velocity intervals less than 0.25 km s^{-1}. To effectively illustrate these features in the new data, we show the channel images of the ^{12}CO and ^{13}CO J = 2−1 emission in Figs 1 and 2, respectively. In the ^{12}CO images, the striations appear in each displayed velocity interval and are mostly parallel to each other. The blueshifted features are generally fainter and narrower than the redshifted counterparts. Striations are evident within the core velocity interval ($6.3 < V_{\rm LSR} < 6.7$ km s^{-1}) but with less contrast with respect to brighter diffuse emission component. The ^{13}CO J = 2−1 emission is very weak in this field. The detected signal resides within the redshifted half of the line profiles and is mostly distributed within an extended component. There are faint, elongated features that align with the brightest ^{12}CO striations within the $V_{\rm LSR}$= 7.38 and 7.72 km s^{-1} images.

Assuming spinning, elongated dust grains with minor axes aligned with the magnetic field, we calculate the local mean magnetic field direction from the set of 18 optical/IR polarization angles located within 1 deg of our field centre from the compilation by Heiles (2000). The mean angle is 36° with a standard deviation of 7° indicating that the projected magnetic field is highly uniform in this sector of the Taurus cloud. This mean angle is comparable to the value of 27° derived from 353 GHz polarization of dust emission from the approximate centre of our map (Planck Collaboration XXXV 2016). Fig. 1 shows the alignment of the brightest striations along the local magnetic field direction inferred from the optical/IR polarization.

The spatial variation of the Taurus striations with velocity motivates an examination of the molecular line profiles within this field. Spectrograms (position–velocity images) are constructed from the ^{12}CO and ^{13}CO J = 2−1 and J = 1−0 data cubes along an axis running perpendicular to the striations, as illustrated by the trapezoid shown in each channel image of Fig. 1. The long axis of the trapezoid corresponds to the length of the spectrogram. Spectra are averaged along the width of the trapezoid to gain signal to noise in the final spectrogram. This width narrows along the length of the trapezoid due to the confines of the observed field so the resultant noise level is not constant along the spectrogram. The spectral axes of each spectrogram are aligned to facilitate the calculation of isotopic and line ratios. The rms noise levels per channel are 0.014, 0.012, 0.14, and 0.066 K for the ^{12}CO J = 2−1, ^{13}CO J = 2−1, ^{12}CO J = 1−0, and ^{13}CO J = 1−0 spectrograms, respectively. The spectrogram lengths for each data set are converted into parsecs assuming a distance to the Taurus molecular cloud of 140 pc.

The spectrograms for each transition and isotopologue are shown in Fig. 3. There is a clear periodic pattern in the ^{12}CO J = 2−1 and J = 1−0 spectra, which is not detected in either ^{13}CO spectrograms. Excess emission oscillates between the blue and red shoulders of the line profile along the spectrogram axis. This effect is also seen in the variation of the velocity centroid and skewness of the spectrogram line profiles. The overlayed sine waves, guided by the ^{12}CO J = 2−1 data, are drawn to illustrate these velocity oscillations. For offset positions less than 0.9 pc, the data are well described by a single sine wave with a projected wavelength of 0.23 pc. For the fainter features with offset positions greater than 0.9 pc, the velocity

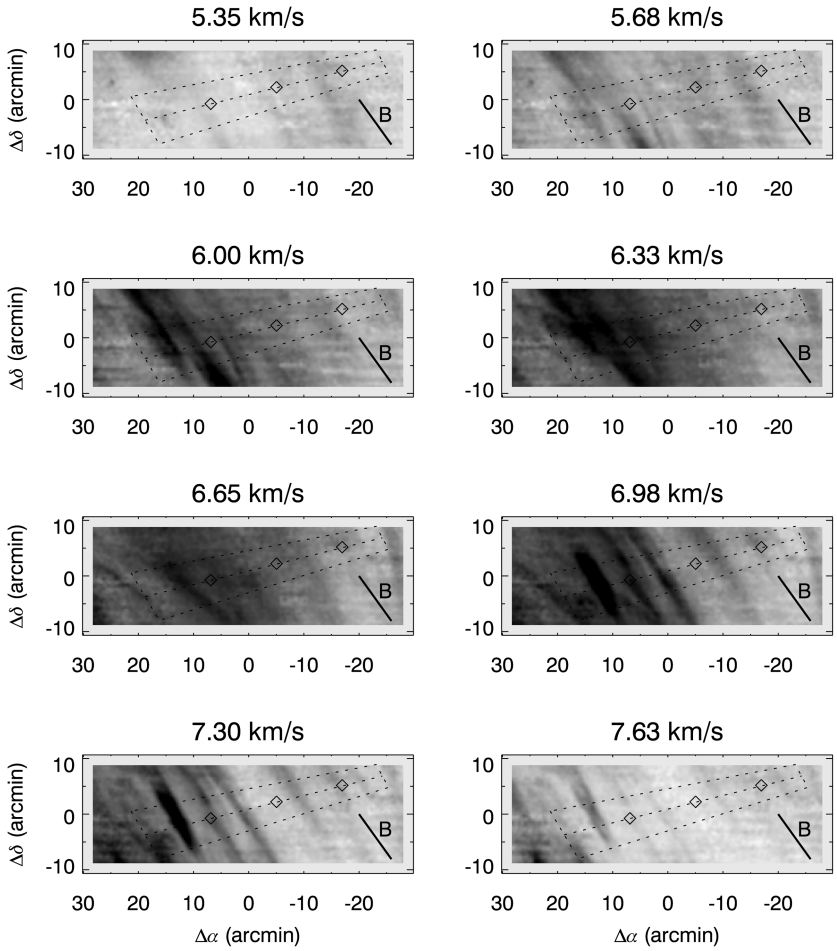

Figure 1. Images of ^{12}CO J = 2−1 emission within separate spectroscopic channels. Halftones range from −0.2 K (white) to 2 K (black). The black line segment indicates the local magnetic field direction inferred from optical/IR polarization vectors. The trapezoid shapes in each image show the length over which the spectrogram in Fig. 3 are constructed and the width over which spectra are averaged. The diamond symbols along the central axis of the trapezoid denote lengths measured from the left edge of 0.5, 1, and 1.5 pc. Striations are evident in all channels but the first.

pattern shifts in phase and increases in wavelength to 0.3 pc. These quasi-periodic velocity oscillations lead to the interleaving of the brightest blueshifted striations ($5.35 < V_{\rm LSR} < 6\,{\rm km\ s^{-1}}$) with the brightest, redshifted striations ($7.0 < V_{\rm LSR} < 7.6\,{\rm km\ s^{-1}}$) shown in Fig. 1.

Establishing the physical conditions of the gas within and between the striations for a given velocity interval can help guide a description of the physical origin of these features. Do the striations correspond to sites of enhanced volume density, warmer gas temperatures, and larger CO abundances relative to the background as may be expected for a shock, instability, or longitudinal MHD wave? Ideally, the set of observed CO lines offers limited constraints on the physical conditions within the observed field. Since the spatial variations of the emission are a strong function of velocity, we first examine the J = 2−1 to J = 1−0 line ratios in individual velocity channels along the spatial extent of the ^{12}CO and ^{13}CO spectrograms as shown in Fig. 4. The rms errors for each transition are propagated to derive an uncertainty in the ratio. For clarity, only ratios with signal to noise greater than 5 are displayed. The trace of the J = 2−1 antenna temperature for each velocity interval, $T_{\rm mb}(v)$, is also drawn to place the line ratio in context with the striations. Fig. 4 illustrates that there is detected ^{12}CO J = 2−1 emission at all positions along the spectrogram lengths. The striations are enhancements of signal relative to this background component. The fractional increments of the striations relative to the background signal varies with position and velocity – ranging from 10 to 100 per cent with the strongest boost in the $V_{\rm LSR} = 6.98$ and $7.30\,{\rm km\ s^{-1}}$ channels. Overall, there is no clear relationship between the measured line ratios and striation locations. There are both small ratio increments and decrements at the striation positions and within the gaps between the striations. The ^{12}CO line ratios profiles are flat within the core of the line (6.33 and $6.65\,{\rm km\ s^{-1}}$ channels). The ratio derived from the lower opacity ^{13}CO lines should be more sensitive to local density variations. Yet, the ^{13}CO ratios are also flat along the length where the ratios are reliably measured.

While the observed 2−1/1−0 line ratios are evidently not sensitive enough to measure variations in temperature and density within the narrow velocity range of the striations, the range and mean values do provide a coarse measure of the average physical conditions in the field. Average spectra for each isotopologue and transition are constructed from the data cubes using equal weighting. Integrated intensities are calculated from these average spectra over the velocity interval 4.5 to $8\,{\rm km\ s^{-1}}$. The corresponding 2−1/1−0 line ratios are 0.68 and 0.34 for ^{12}CO and ^{13}CO, respectively with propagated random errors less than 1 per cent. Gaussian profiles are fit to each average spectrum to determine the peak intensity and

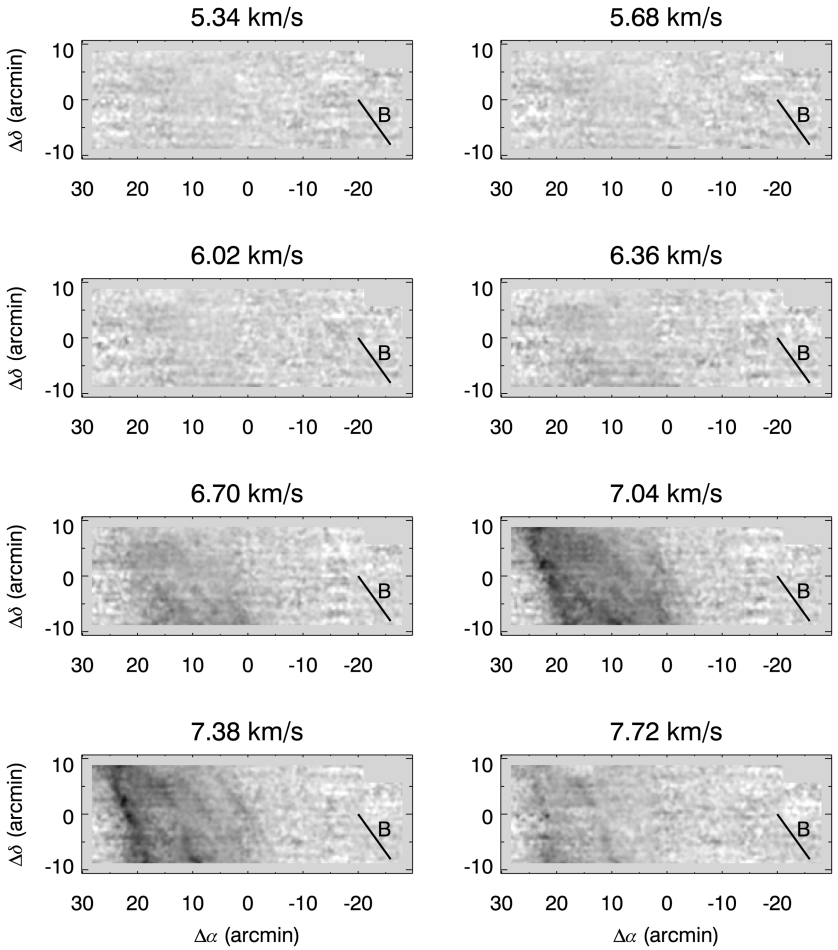

Figure 2. Images of ^{13}CO J = 2−1 emission within separate spectroscopic channels. Halftones range from −0.15 K (white) to 0.75 K (black).

the full width at half-maximum line width, δv that are required for non-local thermodynamic equilibrium (non-LTE) modelling. Peak antenna temperatures are 1.3 K and 1.9 K for the ^{12}CO J = 2−1 and J = 1−0 lines, respectively; and 0.14 K and 0.45 K for the ^{13}CO J = 2−1 and J = 1−0 transitions. The deconvolved, 1D, full width half-maximum line widths are 1.7 km s^{-1} for the ^{12}CO lines and 0.7 km s^{-1} for the ^{13}CO lines.

The line radiative transfer and excitation model, RADEX (van der Tak et al. 2007), is used to compute model line ratios and intensities for a set of cloud conditions (temperature, density, column density). With two transitions and two isotopologues, we might hope to identify a simple set of cloud conditions for which the non-LTE model matches the measured line ratios and brightness temperatures. However, this is not the case. The primary impediment to a self-consistent model is the large line ratio and low-brightness temperature of ^{12}CO, and simultaneously, low ^{13}CO line ratio.

A simple argument can be made for unresolved, inhomogeneous density structure in the Taurus envelope that can explain the observed line ratios. There is a family of model cloud conditions that are consistent with the line ratio of the optically thin ^{13}CO lines. For example, models with kinetic temperature and volume density, $(T_k, n) = (10\,\mathrm{K}, 880\,\mathrm{cm}^{-3})$, $(20\,\mathrm{K}, 330\,\mathrm{cm}^{-3})$, and $(30\,\mathrm{K}, 210\,\mathrm{cm}^{-3})$, all match the mean ^{13}CO 2−1/1−0 line ratio of 0.34. Using any of these density and temperature combinations does not produce the larger observed ^{12}CO 2−1/1−0 line ratio of 0.68 unless the optical depths of the ^{12}CO lines are sufficiently large for radiative trapping to increase the excitation of ^{12}CO relative to ^{13}CO. Although ^{12}CO is subthermally excited, any model that matches the observed ^{12}CO line ratio predicts line intensities ∼5 times larger than observed. This difference between the modelled and observed line intensities can be removed if much of the CO emission originates in a medium composed of unresolved substructures, hereafter cells, that fill a fraction (∼20 per cent) of the antenna beam area at any velocity. Such small scale density or abundance inhomogeneities in molecular clouds have been inferred by previous studies based on similar excitation arguments as those described here (Goldsmith, Plambeck & Chiao 1975; Snell et al. 1984; Tauber, Goldsmith & Dickman 1991; Falgarone & Phillips 1996; Falgarone et al. 1998; Hily-Blant & Falgarone 2007). Falgarone & Phillips (1996) derive an upper limit to the size of cells in the envelope of the Perseus–Auriga cloud to be 34 au based on the smoothness of line profiles observed with high signal to noise and the requirement of moderate beam averaged optical depths. With only two CO isotopologues, two rotational transitions, and moderate signal to noise, we cannot establish any more precisely the conditions, sizes, or the number of cells in this part of the Taurus cloud.

The clumpy medium description of the cloud envelope gas implied by the modelling of the line ratios and intensities offers an alternative view of the striation molecular emission. The variation of ^{12}CO surface brightness across the spectrogram axis results from the spatial modulation of the beam filling factor of unresolved cells at a given velocity rather than changes of the excitation conditions.

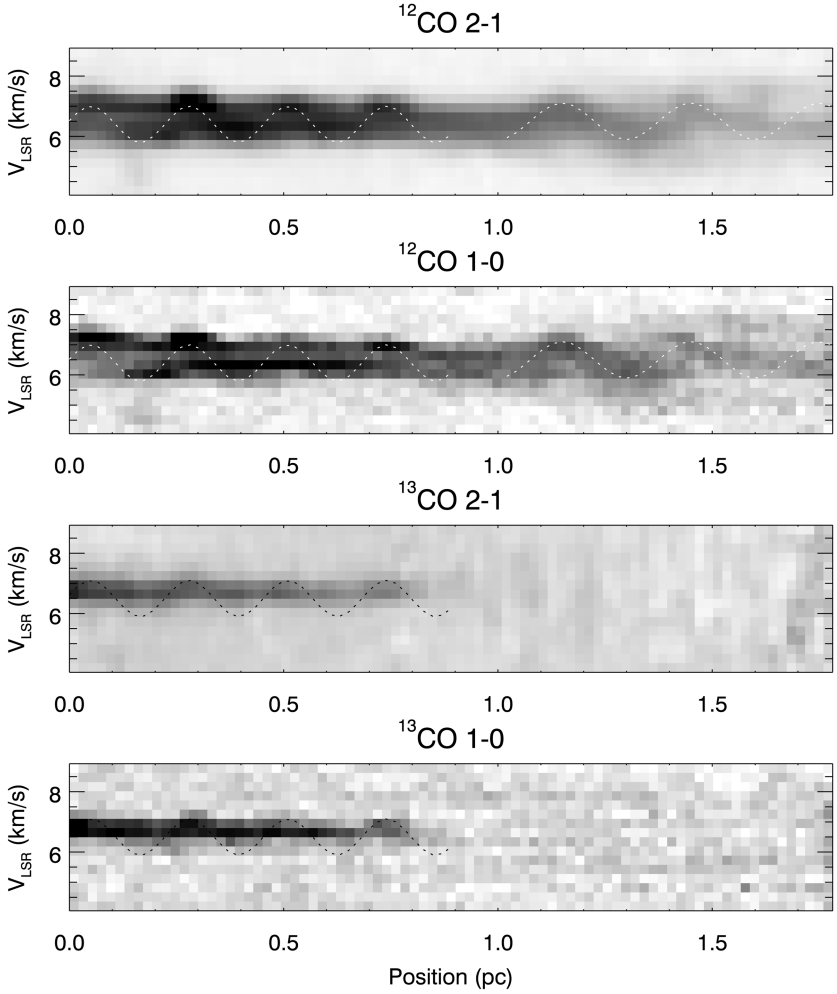

Figure 3. Spectrograms along an axis perpendicular to the striations and local magnetic field direction for (top to bottom) ^{12}CO J = 2−1, ^{12}CO J = 1−0, ^{13}CO J = 2−1, and ^{13}CO J = 1−0. The corresponding halftone ranges are: −0.1 K (white) to 2.0 K (black); −0.2 K (white) to 3.0 K (black); −0.1 K (white) to 0.5 K (black); −0.15 K (white) to 1.0 K (black). The dotted lines are 'by-eye' fits of sine waves to oscillating excess emission in the blue and redshifted shoulders of the line profiles. These velocity oscillations lead to the interleaving of the blue and redshifted striations.

The observed invariance of the line ratios reflects the uniformity of temperature and density within the cells. The physical mechanisms responsible for this modulation of filling factor and velocity are discussed in Section 4.

4 DISCUSSION

The data described in the previous section and the results from earlier studies point to the magnetic field as the responsible agent for the aligned striations in the envelope of the Taurus molecular cloud. The improved signal to noise of the J = 2−1 data, relative to the J = 1−0 data, identifies a quasi-periodic pattern of ^{12}CO emission that switches between the blue and the red shoulders of the observed line profiles as shown in Fig. 3. This oscillatory velocity behaviour produces the interleaving of the blue and redshifted striations with each other. The other key characteristic of the striations is the anisotropy of velocities in this region (Heyer et al. 2008; Heyer & Brunt 2012). Velocity profile shapes and centroid velocities vary smoothly, if at all, along the length of the striations and magnetic field. Perpendicular to these directions, the molecular gas velocities exhibit higher spatial frequency variations, as demonstrated in Fig. 3. This magnetically aligned velocity anisotropy is only possible in a medium for which the gas motions are sub-Alfvénic (Heyer et al. 2008; Esquivel & Lazarian 2011). Modelling of the line ratios and intensities of the J = 2−1 to J = 1−0 transitions suggests the medium is inhomogeneous and that the CO emission from the striations is enhanced above the background due to an increased filling factor of small, unresolved condensations within the beam.

The ^{12}CO striations are unlikely due to hydrodynamic shocks. First, there is no signature of a strong density enhancement that would be expected from an isothermal or adiabatic shock. Given the orientation of the striations, a shock would be produced by flows moving perpendicular to the magnetic field. Yet, there is no curvature in structure of the magnetic field. Such flow would have to be broadly distributed and spatially coherent to produce such a planar shock front. Finally, such shocks would not produce the interleaved pattern of blue and redshifted features.

4.1 Kelvin–Helmholtz Instability

The regular sequence of the brightest striations could be the product of the K-H instability that arises along the interface of two contiguous layers with different tangential velocities and volume densities. In the Taurus envelope, such layers could be two contiguous,

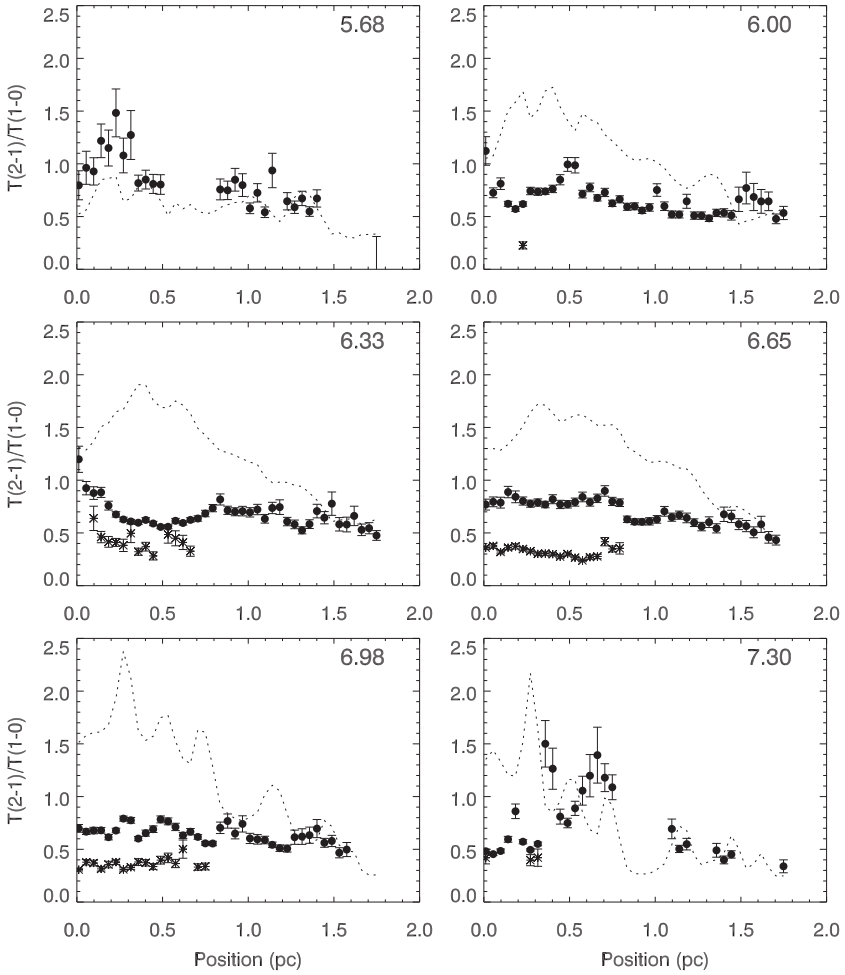

Figure 4. Variation of antenna temperature ratios ($T_{\rm mb}(2-1)/T_{\rm mb}(1-0)$), for ^{12}CO (solid circles) and ^{13}CO (asterisk) along the spectrogram axis. The dotted line corresponds to the ^{12}CO J = 2−1 brightness temperature for each velocity channel. There is no correspondence between positions of enhanced excitation and the location of the striations.

turbulent eddies or the interface between warm, neutral atomic gas and cold, neutral material. The K-H instability produces alternating zones of high and low pressure that correspond to sites of higher and lower gas density. For a clumpy medium, this could be reflected in the periodic variation of the beam filling fraction of dense cells inferred from the line ratios.

Berné & Matsumoto (2012) and Hendrix et al. (2015) examined the role of the magnetic K-H instability in producing the ripples of dust emission observed near the interface of the H II region and molecular cloud in Orion (Berné, Marcelino & Cernicharo 2010). In their model, the interface is in the x–z plane, the velocity and density gradients are along the y-axis, and the magnetic field is at angle θ to the z-axis. The spacing of the Orion ripples falls within the range of instability wavelengths (0.06–0.6 pc for the conditions in Orion) but only if $|\theta| < 25^\circ$. Viewed from a line of sight along the y-axis (viewing the x–z plane), one would observe periodically spaced ripples along the x-axis that stretch vertically along the magnetic field direction (z-axis). Magnetic fields oriented transverse to the flow direction do not impact the wavelength or growth rate of the K-H instability (Chandrasekhar 1961).

The environment of the Taurus striations is distinct from that of the region of the Orion ripples. In Orion, the two layers are hot, ionized, low-density gas and cold, dense molecular gas, respectively, and the flow velocities are ∼10 km s^{-1}. In the Taurus envelope, the density and velocity differences are small, based on the limited variation of the CO 2−1/1−0 line ratios and the observed velocity dispersion (∼0.7 km s^{-1}). For two layers with densities ρ_1 and ρ_2, and velocities, u_1 and u_2, the maximum allowed wavelength of the K-H instability limited by gravity is

$$\lambda_{\rm KH,max} = \frac{2\pi}{g}\frac{\alpha_1\alpha_2}{\alpha_1-\alpha_2}(u_1-u_2)^2, \quad (1)$$

where $\alpha_1 = \rho_1/(\rho_1+\rho_2)$, $\alpha_2 = \rho_2/(\rho_1+\rho_2)$, and g is the acceleration due to gravity (Chandrasekhar 1961). Normalizing to the Taurus envelope conditions

$$\lambda_{\rm KH,max} = 6.1\left(\frac{2\times10^{21}\ {\rm cm}^{-2}}{N_{\rm H}}\right)\left(\frac{\alpha_1(1-\alpha_1)}{2\alpha_1-1}\right) \times\left(\frac{(u_1-u_2)}{0.7\ {\rm kms}^{-1}}\right)^2\ {\rm pc}, \quad (2)$$

where we have taken $g = \pi {\rm G}\mu m_{\rm H} N_H$. For these conditions, the observed striations are well within this wavelength upper limit unless α_1 approaches unity. For instabilities developing at the interface between layers of warm (WNM) and cold neutral (CNM) gas, the density contrast can be much higher. Taking fiducial volume density values of 0.5 cm^{-3} and 50 cm^{-3} for the WNM and CNM, respectively, and a velocity difference between the layers of ∼3 km s^{-1}, then $\lambda_{\rm KH,max}$ reduces to ∼1 pc.

The K-H instability supports the appearance of multiple wavelengths, as observed in the target field in Taurus as long as $\lambda < \lambda_{KH,max}$. Using 3D simulations of the magnetic K-H instability, Matsumoto & Seki (2007) found that the local vortices become turbulent at later times. This non-linear behaviour causes these regions to fragment into even narrower features and could qualitatively describe the very small spacing between the striations that are evident in the V_{LSR}= 5.68 km s^{-1} image of Fig. 1.

While the K-H instability can replicate the general appearance of the Taurus striations, (see fig. 8 in Hendrix et al. 2015), two questions must be considered. First, what is the Alfvénic Mach number of the differential flows required for the instability? For gas flows with a component perpendicular to the magnetic field that is super-Alfvénic, one would expect large-scale distortions of the field geometry. Yet, the magnetic field in this part of the Taurus cloud appears uniform over angular scales of 1–2 deg (Planck Collaboration XXXV 2016). Thus, any flows responsible for triggering the K-H instability in Taurus must be sub-Alfvénic. Secondly, can the K-H instability produce the periodic velocity pattern illustrated in Fig. 3? In the 3D MHD simulations of Matsumoto & Seki (2007) with the ratio of gas pressure to magnetic pressure equal to 0.1, the velocity field shows converging streamlines towards the high-pressure zones and more circulatory motions around the low-pressure vortex. The converging flows must be asymmetric in density or temperature to generate a velocity displacement to lower or higher velocities. Such asymmetry must vary periodically to produce the spatially interleaved blue and redshifted striations while also be coherent along the striations to account for the observed anisotropy.

4.2 MHD waves

The concept of gas motions in molecular clouds being a result of propagating hydromagnetic waves was introduced by Arons & Max (1975). Mouschovias et al. (2011) derive the dispersion relationships and describe the allowed modes for MHD waves propagating parallel and perpendicular to the local magnetic field direction as well as the more general case of an arbitrary angle. The two primary modes relevant to this study are neutral transverse Alfvén and neutral magnetosonic waves. The orientation of the striations relative to the local magnetic field, the periodic velocity structure perpendicular to the field, and the absence of velocity structure along the field excludes the neutral, transverse, Alfvén wave as the cause of the striations. Such transverse disturbances produce velocity fluctuations along the striations, while also distorting the local field direction.

If MHD waves are responsible for the striations, then these must be longitudinal magnetosonic waves. As such waves propagate perpendicular to the mean magnetic field direction, the gas and magnetic field are alternately compressed and rarified. In the case of a clumpy medium, the wave disturbance modulates the beam filling factor as oscillating thermal and magnetic pressure displace the cells. The effect is to vary the number of cells within a velocity interval over the solid angle of the telescope beam or resolution element. The striations appear over lengths at which the velocities are coherent in response to the longitudinal disturbance. This wave-induced spatial coherence of velocity along a given striation naturally accounts for magnetically aligned velocity anisotropy that is expressed as different indices of the velocity structure functions calculated parallel and perpendicular to the local field (Heyer et al. 2008; Heyer & Brunt 2012).

MHD waves propagating within molecular clouds are expected to have a limited range of wavelengths owing to neutral–ion gas coupling and gravity (Mouschovias et al. 2011). An upper limit to the wavelength is set by the magnetic Jeans length, $\lambda_{J,mag}$,

$$\lambda_{J,mag} = 2\pi v_{ms,n}\tau_{ff}, \tag{3}$$

where $v_{ms,n} = (v_{A,n}^2 + c_n^2)^{1/2}$ is the magnetosonic speed for neutral gas, $v_{A,n} = B/(4\pi\rho)^{1/2}$ is the Alfvén velocity for neutral gas with mass density ρ, $c_n = 0.27(T/20\,K)^{1/2}$ km s^{-1} is the thermal sound speed, and $\tau_{ff} = (4\pi G\rho)^{-1/2} = 0.8(500\,cm^{-3}/n_H)^{1/2}$ Myr is the free-fall time. This results in

$$\lambda_{J,mag} = 4.8\left(\frac{B}{15\mu G}\right)\left(\frac{500\,cm^{-3}}{n_H}\right) \times \left[(1 + 0.08\left(\frac{T}{20K}\right)\left(\frac{15\mu G}{B}\right)^2\left(\frac{n}{500\,cm^{-3}}\right)\right]^{1/2} \text{pc}. \tag{4}$$

For disturbances with wavelengths larger than $\lambda_{J,mag}$, the gravitational force is larger than the magnetic force and the localized region collapses (Mouschovias 1991).

A minimum wavelength is imposed by the need for frequent neutral–ion collisions to transfer the magnetic force to the bulk of the material (Kulsrud & Pearce 1969; Arons & Max 1975). From the dispersion relations derived by Mouschovias et al. (2011), the minimum wavelength for a neutral, magnetosonic wave is

$$\lambda_{ms,n} = \lambda_{A,n}\frac{v_{A,n}}{v_{ms,n}}, \tag{5}$$

where $\lambda_{A,n}$ is the Alfvén length (Mouschovias 1991). For an electron fraction, x_i,

$$\lambda_{A,n} = \pi v_{A,n}\tau_{ni} = 0.02\left(\frac{B}{15\mu G}\right)\left(\frac{500\,cm^{-3}}{n_H}\right)^{3/2}\left(\frac{10^{-5}}{x_i}\right) \text{pc}, \tag{6}$$

where τ_{ni} is the neutral–ion collision time. For magnetosonic disturbances with wavelengths less than $\lambda_{ms,n}$, the magnetic field diffuses through the neutrals on time-scales shorter than the neutral–ion collision time leaving the neutral particles uncoupled to the magnetic field. In this regime, the wave is rapidly damped (Mouschovias 1991).

The column density, N_H, in the observed field is low (1–2 $\times$ 10^{21} cm^{-2}) based on infrared-derived extinction and CO column densities (Pineda et al. 2010). In this regime, both far-UV radiation and cosmic rays contribute to the gas ionization. Using the Meudon PDR Model (Le Petit et al. 2006), we have calculated the ionization fraction with the following primary model parameters: radiation field of 1 Mathis field illuminated from both sides of the slab, a hydrogen density of 500 cm^{-3}, a maximum depth of 3 A_v, and a cosmic ray ionization rate of 5 $\times$ 10^{-17} s^{-1}. The resultant electron fraction at a depth of 2 mag, measured from the front face of the cloud, is 7.8$\times$10^{-5}. In this low volume density, diffuse environment, the minimum wavelength could be as small as 0.01 pc.

The projected wavelength for the brightest, and most repetitive striations in the V_{LSR} = 6.98 km s^{-1} channel is 0.23 pc. As the striations are likely in a plane inclined to the plane of the sky by angle, θ_i, the actual wavelength is 0.23/cos(θ_i) pc. Even accounting for these projections, the striations satisfy the wavelength conditions, $\lambda_{ms,n} < \lambda < \lambda_{J,mag}$.

While the observed wavelengths comply with the restrictions imposed by gravity and neutral–ion collision times, the magnetosonic waves do not fully account for the observations. For a sinusoidal variation of gas spatial displacement, s = s$_{max}$cos(kx $-$ ωt), caused

by the longitudinal wave disturbance, the velocity and density (beam filling factor) vary as $\partial s/\partial t$ and $\partial s/\partial x$, respectively, where s_{max} is the maximum displacement, $k = 2\pi/\lambda$ and ω is the angular frequency of the wave. Density or beam filling fraction and velocity maxima, which may be related to the striations, occur when $kx - \omega t = n\pi$ and n is an even integer, while density and velocity minima occur when n is an odd integer. Depending on the direction of the wave propagation (sign of k) and the angle of propagation with respect to the plane of the sky (since we only measure the radial component of the velocity shift), one expects a correspondence between the maximum velocity and maximum density (beam filling factor). Similarly, there should be minima in the density (beam filling factor), where the velocity is minimum. Such a condition is only partially observed as the striations occur at both blue and redshifted velocities. Evidently, interstellar gas flows are more complicated than the idealized, single wave disturbance discussed here.

4.3 MHD waves and K-H instabilities in molecular clouds

With the current data, we cannot definitely assign either the K-H instability or magnetosonic waves as the physical origin of the Taurus striations. Both processes qualitatively produce such features aligned along the local magnetic field direction and predict density enhancements or increased beam filling fractions at the positions of the striations. The observed projected wavelengths of the striations are smaller than the wavelength upper limits set by gravity for both the K-H instability and wave disturbance and larger than the minimum wavelength imposed by neutral–ion collision frequency. The oscillatory behaviour of the line profiles can be partially reproduced by a magnetosonic wave propagating transverse to the local field direction but inclined to the plane of the sky. Compression and rarefaction of the gas, represented by beam filling fraction, corresponds to the peak and trough of the wave depending on the direction and inclination of the wave propagation. The wave model also describes the magnetically aligned velocity anisotropy.

The striations are not isolated to this small subregion within the Taurus cloud. Wispy structures with similar velocity anisotropy aligned along the local field direction are found throughout the low column density regime of the Taurus cloud (Heyer & Brunt 2012). The identification of these striations within the cloud envelope likely results from a favourable viewing angle, a well-resolved wavelength of a single disturbance, and a relatively limited depth into the cloud. In the high column density regions of the cloud, corresponding to higher surface brightness CO emission, such striations are not apparent due to several factors. In this regime, such features are masked by brighter emission from other structures along the line of sight and the beam area filling fraction within a small velocity interval approaches unity offering little or no contrast. For the K-H instability, the maximum allowed wavelength would be smaller owing to increased column density and reduced turbulent velocity differences at smaller scales. Similarly, only smaller wavelength magnetosonic modes are allowed in regions of high volume density and reduced ionization. At some point, such features are not resolved by the moderate angular resolution of these data. Finally, waves propagating from different directions can interact with each other in the central regions of the cloud. Such interactions can distort any simple, recognizable pattern of an isolated wave.

In a more general context, the presence of magnetosonic waves and K-H instabilities, revealed by striations, should be common mechanisms in any sub-Alfvénic molecular cloud threaded by the interstellar magnetic field with sufficient ionization to couple the neutral gas to ions. Indeed, striations are observed throughout the cold, neutral interstellar medium (ISM) in the dust emission maps of *IRAS*, *Herschel*, and *Planck* missions and imaging of the H I 21 cm line (Clark, Peek & Putman 2014). Many of these low column density filamentary features are aligned with the local magnetic field direction (Planck Collaboration XXXV 2016). The ubiquity of striations throughout the cold, neutral ISM, generated by K-H instabilities and/or magnetosonic waves illustrates an important role of the interstellar magnetic field in modulating gas motions.

5 CONCLUSIONS

^{12}CO and ^{13}CO J = 2−1 data collected by the ARO 10-m telescope are analysed in conjunction with available J = 1−0 data to investigate the nature of striations that are aligned along the magnetic field in the Taurus molecular cloud. The high sensitivity of the J = 2−1 data identify spatially oscillating blue and red shoulder line profile components corresponding to the striations. A medium comprised of unresolved cells that are responsible for the CO emission is inferred from the ^{12}CO and ^{13}CO 2−1/1−0 line ratios and intensities. The striations result from the modulation of the velocities and the beam area filling faction of the cells by either a K-H instability or magnetosonic waves propagating through the envelope of the Taurus cloud. Such processes may explain the appearance of similar striations observed throughout the cold, neutral ISM in images of dust and gas emission.

ACKNOWLEDGEMENTS

The authors thank L. Ziurys for granting additional time at the ARO to improve the sensitivity of the data and J. Bieging for guidance on calibration of the data. The Heinrich Hertz Submillimeter Telescope is operated by the ARO, which is part of Steward Observatory at The University of Arizona. The ARO is funded in part by National Science Foundation grant AST-1140030 to The University of Arizona.

REFERENCES

Arons J., Max C. E., 1975, ApJ, 196, L77
Basu S., Dapp W. B., 2010, ApJ, 716, 427
Berné O., Matsumoto Y., 2012, ApJ, 761, L4
Berné O., Marcelino N., Cernicharo J., 2010, Nature, 466, 947
Carlberg R. G., Pudritz R. E., 1990, MNRAS, 247, 353
Chandrasekhar S., 1961, Hydrodynamic and hydromagnetic stability. Clarendon, Oxford
Chandrasekhar S., Fermi E., 1953, ApJ, 118, 113
Chapman N. L., Goldsmith P. F., Pineda J. L., Clemens D. P., Li D., Krčo M., 2011, ApJ, 741, 21
Clark S. E., Peek J. E. G., Putman M. E., 2014, ApJ, 789, 82
Esquivel A., Lazarian A., 2011, ApJ, 740, 117
Falgarone E., Phillips T. G., 1996, ApJ, 472, 191
Falgarone E., Puget J.-L., Perault M., 1992, A&A, 257, 715
Falgarone E., Panis J.-F., Heithausen A., Perault M., Stutzki J., Puget J.-L., Bensch F., 1998, A&A, 331, 669
Gehman C. S., Adams F. C., Watkins R., 1996, ApJ, 472, 673
Goldsmith P. F., Plambeck R. L., Chiao R. Y., 1975, ApJ, 196, L39
Goldsmith P. F., Heyer M., Narayanan G., Snell R., Li D., Brunt C., 2008, ApJ, 680, 428
Heiles C., 2000, AJ, 119, 923
Hendrix T., Keppens R., Camps P., 2015, A&A, 575, A110
Heyer M. H., Brunt C. M., 2004, ApJ, 615, L45
Heyer M. H., Brunt C. M., 2012, MNRAS, 420, 1562
Heyer M., Gong H., Ostriker E., Brunt C., 2008, ApJ, 680, 420
Hily-Blant P., Falgarone E., 2007, A&A, 469, 173

Kulsrud R., Pearce W. P., 1969, ApJ, 156, 445
Langer W. D., 1978, ApJ, 225, 95
Larson R. B., 1981, MNRAS, 194, 809
Le Petit F., Nehmé C., Le Bourlot J., Roueff E., 2006, ApJS, 164, 506
Matsumoto Y., Seki K., 2007, J. Geophys. Res.: Space Phys., 112, 6223
Mouschovias T. C., 1991, ApJ, 373, 169
Mouschovias T. C., Ciolek G. E., Morton S. A., 2011, MNRAS, 415, 1751
Narayanan G., Heyer M. H., Brunt C., Goldsmith P. F., Snell R., Li D., 2008, ApJS, 177, 341
Pineda J. L., Goldsmith P. F., Chapman N., Snell R. L., Li D., Cambrésy L., Brunt C., 2010, ApJ, 721, 686
Planck Collaboration XXXV, 2016, A&A, 586, A138
Snell R. L., Mundy L. G., Goldsmith P. F., Evans II N. J., Erickson N. R., 1984, ApJ, 276, 625
Tauber J. A., Goldsmith P. F., Dickman R. L., 1991, ApJ, 375, 635
van der Tak F. F. S., Black J. H., Schöier F. L., Jansen D. J., van Dishoeck E. F., 2007, A&A, 468, 627

This paper has been typeset from a TEX/LATEX file prepared by the author.